Tampere University

Jani Ahvenjärvi

INTERFEROMETRIC AUTOCORRELATION MEASUREMENT OF SUPERCONTINUUM USING TWO-PHOTON ABSORPTION

Bachelor's thesis
Faculty of Engineering and Natural Sciences
Examiner: Prof. Goëry Genty
October 2020

ABSTRACT

Jani Ahvenjärvi: Interferometric autocorrelation measurement of supercontinuum using two-photon absorption
Bachelor's thesis
Tampere University
Engineering and Natural Sciences
October 2020

Supercontinuum (SC) light is a promising light source for a wide range of applications due to its unique characteristics which combine laser light properties with a broad spectrum. Different applications generally require different coherence properties and it is therefore important to characterise them. The first-order coherence properties of SC light have been studied extensively but knowledge of the second-order (intensity) coherence properties are also needed to fully characterize the SC coherence.

In this thesis, we use an interferometric autocorrelation based on two-photon absorption in a GaP photodetector to measure the second-order coherence properties of a SC generated by injecting few hundred fs pulses from Ti:Sapphire laser in the anomalous dispersion regime into photonic crystal fiber. The interferometric autocorrelation technique is implemented using a Michelson interferometer and two-photon absorption is ensured in the detector by tight focusing. Alignment is performed using the pulses directly from the Ti:Sapphire and measuring the two-photon absorption signal.

The interferometric autocorrelation method based on two-photon absorption is a promising avenue to measure the second-order coherence properties of the SC compared to the more conventional second harmonic generation based methods which requires complex phase-matching experimental arrangements due to wide spectrum of SC sources. We also discuss possible further improvements to the measurement setup.

Keywords: Coherence, Two-photon absorption, Interferometric autocorrelation, Supercontinuum

TIIVISTELMÄ

Jani Ahvenjärvi: Superjatkumovalon interferometrinen autokorrelaatiomittaus kaksifotoniabsorptiota käyttäen
Kandidaatintyö
Tampereen yliopisto
Teknis-Luonnontieteellinen
Lokakuu 2020

Superjatkumovalo on lupaava valonlähde monien sovelluksien kannalta, sillä se yhdistää ainutlaatuisella tavalla laservalon ominaisuudet ja laajan spektrin. Valonlähteen koherenssiominaisuuksien karakterisointi on tärkeää, sillä koherenssiominaisuudet määräävät valonlähteen sopivuuden erilaisiin sovelluksiin. Ensimmäisen asteen koherenssiominaisuudet superjatkumovalonlähteille ovat laajasti tutkittuja, mutta myös toisen asteen (intensiteetti) koherenssiominaisuuksien määrittäminen tarvitaan superjatkumovalonlähteiden koherenssiominaisuuksien täydelliseen karakterisointiin.

Tässä työssä käytettiin kaksifotoniabsorptioon perustuvaa interferometristä autokorrelaatiota superjatkumovalon toisen asteen koherenssiominaisuuksien määrittämiseen. Superjatkumovalo luotiin fotonikidekuidussa fokusoimalla siihen 200 femtosekunnin pituisia pulsseja titaani-safiirilaserista anomaalisen dispersion alueella. Interferometrinen autokorrelaatio toteutettiin Michelsonin interferometrillä ja kaksi-fotoniabsorptio varmistettiin GaP fotodetektorissa tiukalla fokusoinnilla. Mittalaitteiden suuntaaminen varmistettiin mittaamalla kaksifotoniabsorptiosignaalia suoraan titaani-safiiri-laserista.

Kaksifotoniabsorptiota hyödyntävä interefrometrinen autokorrelaatiomittaus on lupaava vaihtoehto toisen asteen koherenssiominaisuuksien määrittämiseen superjatkumovalonlähteille. Superjatkumovalon laajan spektrin takia tyypilliset taajuuskahdennusta hyödyntävät menetelmät vaativat monimutkaisia mittausjärjestelmiä vaihesovituksen toteuttamiseksi. Työssä on myös ehdotettu mahdollisia parannuksia mittausjärjestelyihin.

Avainsanat: Koherenssi, Kaksi-fotoniabsorptio, Interferometrinen autokorrelaatio, Superjatkumovalo

CONTENTS

1 INTRODUCTION

Supercontinuum (SC) light have unique characteristics of laser light combined with very broad spectrum. Due these features SC have drawn a significant amount of attention with possibilities for a wide range of applications including telecommunication, imaging, sensing, metrology and coherent spectroscopy [1]. However different applications require particular coherence properties of the light. Field correlations of SC have been studied obtaining normalized degree of spectral coherence [2] although also intensity correlations are needed for more complete characterization of the SC coherence properties.

In this thesis the second-order (intensity) coherence properties of supercontinuum light generated in a photonic crystal fiber are investigated using interferometric autocorrelation based on two-photon absorption in a GaP photodetector. The SC light is generated by injecting few hundred fs pulses from Ti:Sapphire laser into a photonic crystal fiber in the anomalous dispersion regime. The SC light is guided to a Michelson interferometer where scanning of the pulse with itself is made using piezo-electric stage. Light from the interferometer is focused to GaP photodetector to ensure two-photon absorption and signal is collected with an oscilloscope.

2 THEORETICAL BACKGROUND

2.1 Supercontinuum generation

Supercontinuum generation refers to the massice spectral broadening of initially narrowband light via a cascade of nonlinear effects. It can be achieved by injecting intense light into a nonlinear material where linear and nonlinear effects interplay. Nonlinear processes in the medium generate new frequency components yielding and wide spectrum. Various effects play an important role in the generation of a supercontinuum and the most important ones are described in this chapter.

2.1.1 Dispersion

Dispersion is an important linear effect that also plays a critical role in nonlinear fiber optics. The total dispersion is the combination of material dispersion and waveguide dispersion. The effect of material dispersion is usually greater than the waveguide dispersion but when dimensions of the waveguide approaches the wavelength and the refractive index difference between the core and the cladding increases leading to waveguide dispersion to increase.

The dependence of the refractive index of the material on frequency of light is referred to as material dispersion. It is caused by interactions of light with electrons in the medium. The medium response varies as a function of frequency causing different velocities and time delays between different frequencies during propagation. As a practical example, this effect leads to a prism separating different wavelengths to different angles to preserve momentum. Material dispersion can not be changed as it is intrinsic property of the material.

Waveguide dispersion is caused by power distribution in the fiber's core and cladding. Shorter wavelength power distribution is more confined to the core than longer wavelengths. Since light travels faster in the core and slower in the cladding shorter wavelengths experience effectively a higher refractive index. The geometry of the waveguide then defines waveguide dispersion, and it can therefore be tuned by proper design[3].

Dispersion can be described as normal or anomalous depending whether longer (or

shorter) wavelengths travel faster than shorter (longer). The wavelength range where the former happens is referred as normal dispersion regime and the latter as anomalous dispersion regime. The wavelength between normal and anomalous dispersion where material and waveguide dispersion cancel each other out is called zero dispersion wavelength (ZDW). The most used material for optical fibers is silica where the ZDW for material dispersion is at 1.3μm. With proper design, the ZDW and anomalous dispersion regimes can be shifted down to the visible wavelengths as is the case for example in photonic crystal fibers. The pump wavelength compared to the ZDW is crucial for determining the dynamics when generating a supercontinuum[4].

2.1.2 Self and cross-phase modulation

Self-phase modulation (SPM) is caused by the Kerr effect which can be described as the intensity dependence of the refractive index. An intense time-varying filed propagating in a Kerr medium induces a change in local refractive index $\Delta n = n_2 I(t)$ where n_2 is nonlinear refractive index of the material and $I(t)$ is the time-varying intensity. Time varying intensity modulates refractive index and results in a time dependent phase shift for the electric field. This leads to the generation of new frequencies in the spectrum while the pulse temporal profile remains unaffected.

When two co-propagating electric fields with different center frequencies experience change in refractive index dependent on the other field via Kerr effect, it is referred as cross-phase modulation (XPM) [5].

2.1.3 Four-wave mixing and modulation instability

Four-wave mixing (FWM) is also caused by the Kerr effect. Two or more optical fields modulate the refractive index via the Kerr effect and can produce new frequency components around the original ones. Key features of the process is seen in the example where two pump waves which have frequencies ν_1 and ν_2 are converted to a pair of side bands around the pump at ν_3 and ν_4. One which is downshifted (Stokes wave) and other which is upshifted (anti-Stokes wave) relative to the pump frequency. This is illustrated in figure 2.1.

In the absence of the initial seeding four-wave mixing is seen as instability of the CW pump and symmetrical sidebands in the frequency domain are grown from noise. It should be noted that FWM and modulation instability (MI) are time- and frequency-domain descriptions of the same physical phenomena [4].

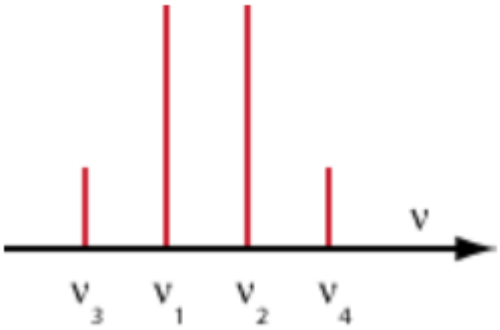

Figure 2.1. *Generation of the new frequencies ν_3 (stokes) ν_4 (anti-Stokes) around initial ν_1 and ν_2 via four-wave mixing process*

2.1.4 Raman scattering

Raman scattering describes an inelastic scattering process between photons and the higher vibrational or rotational energy states of the propagation medium (phonons). As it is inelastic, energy is not conserved in the process. Photon energy is changed and the frequency of the incoming light is shifted.

Shifting to both higher and lower frequencies are possible. In the case where the incoming photon has less energy (longer wavelength) than previosly some of the energy is transferred to phonons. It is referred as anti-Stokes scattering and in the case of already excited phonon giving energy to photon (shorter wavelength) anti-stokes scattering occurs. However, it is worth noting that anti-Stokes scattering is much weaker particularly at low temperatures.

Although spontaneous Raman scattering is a relatively weak process, it can be stimulated by a weak amplitude wave co-propagating with an intense laser beam[4].

2.1.5 Solitons

Solitons are observed when the nonlinear phase shift from SPM is precisely balanced by dispersion leading to a waveform that propagates unchanged in time and frequency. Solitons naturally exist in the anomalous dispersion regime where the phase shift induced by dispersion is opposite to that caused by SPM. Note that the input pulse peak power should be high enough to induce sufficient SPM chirp.

It is also notable that dark solitons exist. They are seen as "missing light" in constant background pulse. For this reason bright soliton is sometimes used to mark the difference between solitons in the anomalous and normal dispersion regime. Unlike bright solitons, dark solitons occur in the normal dispersion regime. Bright solitons are produced by lasers, we concentrate on them and in the following the use of soliton word refers to

bright soliton [6].

Solitons are analytical solutions of the nonlinear-Schrodinger equation and they have shape of the hyperbolic secant:

$$A(z=0,T) = \sqrt{P_0} sech(\frac{T}{T_0}). \tag{2.1}$$

P_0 is the peak power of the soliton and T_0 is its duration related to the full-width at half maximum (FWHM) width by $T_0 = T_{FWHM}/1.763$. One can derive a condition on the input pulse peak power when nonlinear and dispersive effects cancel each other:

$$P_0 = \frac{|\beta_2|}{\gamma T_0^2}, \tag{2.2}$$

where β_2 is the GVD-parameter and γ is nonlinear parameter. If the input peak power is higher than in equation 2.2 higher order soliton is obtained. Higher order solitons have initially an hyperbolic secant shape but, unlike fundamental solitons, they do not propagate undistorted. Higher order solitons undergo periodic changes in both temporal and spectral domains, and eventually recover the initial hyperbolic secant shape. The soliton order is defined by

$$N = \sqrt{\frac{\gamma P_0 T_0^2}{|\beta_2|}}, \tag{2.3}$$

where N=1 correspond to a fundamental soliton while N$>$2 to higher order solitons[4].

2.1.6 Dynamics in different regimes

Supercontinuum generation in fibers can be roughly divided into four different regimes depending on the pulse duration and wavelength compared to the fibres zero-dispersion wavelength (ZDW). Table 2.1 shows the dominant mechanisms in different regimes. Division between short and long pulses is roughly so that picosecond and longer pulses are considered as long pulses while few hundred femtosecond and shorter as short pulses. In between, the dynamics of the supercontinuum generation are a mix between these effects.

Table 2.1. *Mechanisms of supercontinuum generation in different regimes of pulse duration and dispersion*

	Anomalous	**Normal**
Short pulse	Soliton dynamics Dispersive waves	Modulation instability Soliton dynamics
Long pulse	Self-phase modulation Four-wave mixing	Raman scattering Four-wave mixing

2.2 Two-photon absorption

Two-photon absorption (TPA) is a nonlinear absorption process where two incident photons are absorbed "simultaneously" producing excitation to a higher energy state. The energy of the transition is the sum of the two incident photons and photons can have different energies. Excitation generally occurs via a virtual energy state which has a very short lifetime. The finite lifetime of the virtual energy state can be understood from quantum mechanics and Heisenberg's uncertainty principle leads a lifetime $\hbar/E_g$ which is in the order of few femtoseconds for bandgaps in the visible range[7]. Energy diagram of TPA compared to single-photon absorption is illustrated in figure 2.2

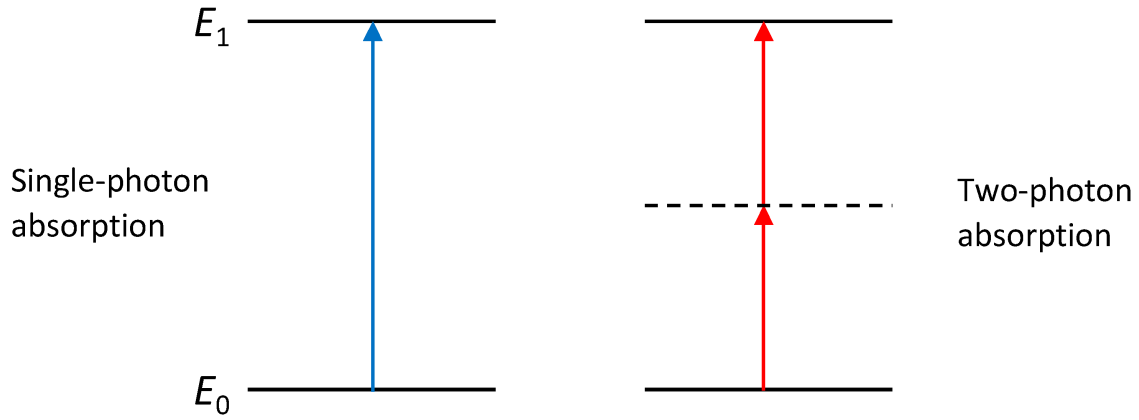

Figure 2.2. *Energy diagram of the single- and two-photon absorption [8]*

In semiconductor materials TPA occurs only when photon energy is $0.5E_g < E < E_g$ so that two photons have combined enough energy to excite electron from the valence band to the conduction band but less than energy of the band gap to avoid single-photon absorption[7].

The change in intensity of light propagating in a material due to both single- and two-photon absorption is given by

$$\frac{\partial I}{\partial z} = -\alpha I - \beta I^2, \tag{2.4}$$

where α and β represent the coefficients for single- and two-photon absorption respectively. Linear absorption is usually order of magnitude larger than TPA so that only at very high intensities TPA is the dominant cause of absorption [9]. Single-photon absorption is directly proportional to the incoming intensity while TPA is proportional to the intensity squared.The dominant absorption process may then be observed by measuring the photo detectors signal vs intensity (power if area is constant). A linear dependency indicates that single-photon absorption dominates while a quadratic dependency marks the dominance of TPA (see chapter 3.3 Detection system).

2.3 Coherence

2.3.1 Temporal and spatial coherence

The correlation between electric fields in two different arbitrary points in the wavefront of light is described by spatial coherence. Spatial coherence is said to be perfect when the electric fields $E_1(t)$ and $E_2(t)$ taken at two different points have constant a phase shift over time for any location in the wavefront. In practice spatial coherence is only preserved over a certain area in the light beam which is called coherence area A_C.

As spatial coherence represents the correlation of electric field between two points in space over time, temporal coherence is correlation of the electric field in one point in space with different times. Let's consider electric field in one point in space but with different time instances t_1 and t_2, if there is constant phase shift between $E(t_1)$ and $E(t_2)$ the temporal coherence is perfect. Temporal coherence is linked to the monochromacity of light. Perfectly monochromatic light is perfectly temporally coherent. In practice however lasers are not perfectly monochromatic with a finite linewidth and temporal coherence is finite. The time interval over which temporal coherence is preserved is called the coherence time τ_c, neglecting the fact that the electric field is fully correlated in the time interval from $E(t)$ to $E(t + \tau_c)$. The temporal coherence is inversely proportional to the linewidth of the light source as $\tau_c = 1/\Delta f$. The distance over which the coherence is preserved is referred to as the coherence length and it is defined as $L_c = \tau_c c$, where c is speed of light[10].

Light sources have their own intrinsic coherence properties which can be modified using external components. For example, the spatial coherence can be increased by using spatial filter such as a pinhole. Similarly, temporal coherence can be increased by filtering wavelengths but this results in a significant loss of power.

2.3.2 Intensity correlation

Second-order temporal correlation function Describes intensity correlations and is defined as

$$G^{(2)}(\tau) = \langle E^*(t)E^*(t+\tau)E(t)E(t+\tau)\rangle. \tag{2.5}$$

For stationary fields the correlation function is generally normalized and it is called the degree of the second order temporal coherence[10]:

$$g^{(2)}(\tau) = \frac{\langle E^*(t)E^*(t+\tau)E(t)E(t+\tau)\rangle}{\langle E^*(t)E(t)\rangle^2}. \tag{2.6}$$

$g^{(2)}$ can be also expressed with the intensities and is referred as intensity correlation:

$$g^{(2)}(\tau) = \frac{\langle I(t)I(t+\tau)\rangle}{\langle I(t)\rangle^2}. \tag{2.7}$$

Normalization is straightforward with stationary light since light average intensity is same at every instant of time and $\langle I(t)\rangle^2$ is constant. Normalization is more complex for non-stationary light such as a pulsed light source where light intensity varies as a function of time.

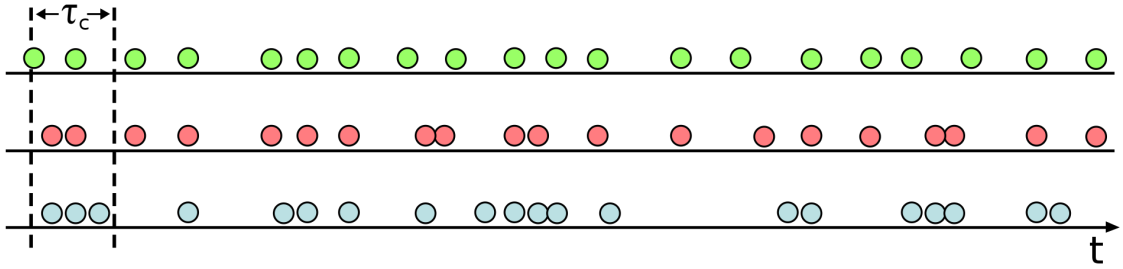

Figure 2.3. *Photon detection as a function of time for anti-bunched, random and bunched light[11]*

Intensity correlation is also linked to photon bunching phenomena and photon statistics. This is illustrated in figure 2.3 which shows photon detection as a function of time. In the bottom row, photons are bunched and more than one photon are emitted "simultaneously". Chaotic light sources such as thermal light sources exhibit bunched photon statistics. Centre row shows no correlation between consecutive photons and photons are emitted randomly. Coherent laser source is a typical example of source with this kind of photon statistics. In the top row decorrelation between emitted photons leads to anti-bunching. Single photon sources exhibit this kind of photon statistics.

The corresponding $g^{(2)}(\tau)$ functions for bunching, random and anti-bunching statistics of photons emitted is shown in figure 2.4. At zero delay $g^{(2)}(\tau)$ reaches 2 for thermal source and reaches values below 1 with anti-bunching. Coherent light source have constant value of 1 and no correlation between emitted photons. It is notable that the coherence time of the source corresponds to the FWHM of the peak at zero delay[13].

2.3.3 Intensity autocorrelation

The most common method for pulse duration measurement is the intensity autocorrelation based on second-harmonic generation. It also possible to use other nonlinear interactions to measure the intensity autocorrelation such as two-photon absorption or two-photon fluorescence. Figure 2.5 shows typical setup for background-free intensity correlation measurement. Using this configuration, the pulse to is divided into two arms

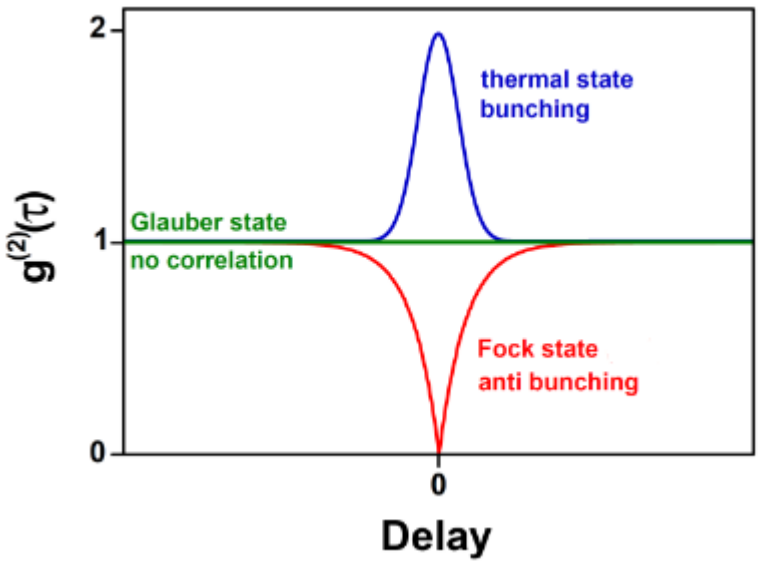

Figure 2.4. *Normalized intensity correlation function states corresponding to probabilities to emit more than one photon at the same time [12]*

and a delay is introduced in one of the arms. Both pulses are focused into a nonlinear crystal. Focusing is achieved non-colinearly such that interference only occurs in the crystal. Second harmonic generation is obtained in the crystal, provided phase-matching is fulfilled. Autocorrelaton trace is obtained by measuring the SHG pulse energy as a function of delay.

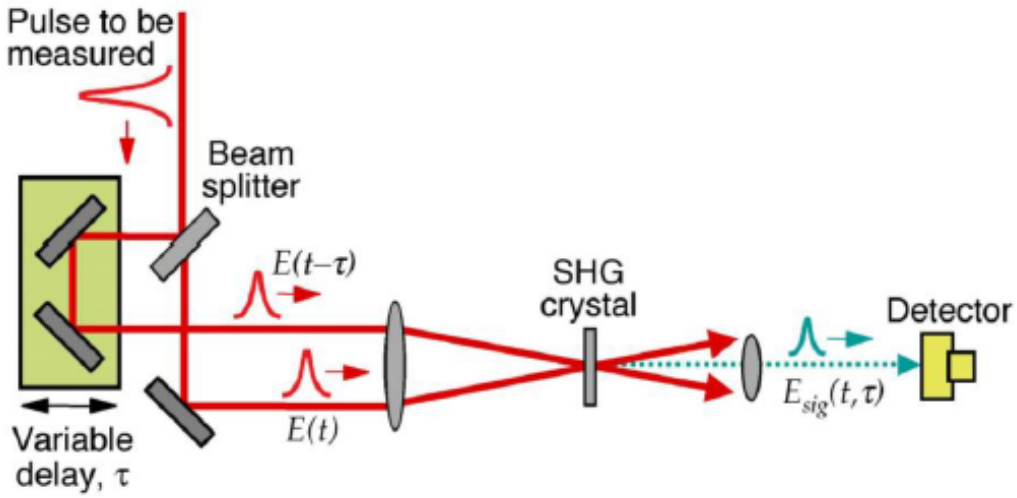

Figure 2.5. *Principle of intensity autocorrelation with SHG [14]*

The nonlinear crystal produces a signal at twice the frequency of the incoming light. The corresponding electric field is given by

$$E(t,\tau) \propto E(t)E(t-\tau) \tag{2.8}$$

where τ is the negative delay between the interfering fields. The intensity of the signal measured is

$$I_{AC}(t,\tau) \propto \int_{-\infty}^{\infty} |E(t)E(t-\tau)|^2 dt = \int_{-\infty}^{\infty} I(t)I(t-\tau)dt \tag{2.9}$$

where integration comes from the fact that response of the photo detector is much slower than the width of the pulse. The autocorrelation trace is zero when the delayed pulses do not overlap in time and is symmetrical with respect to the time delay τ

$$I_{AC}(\tau) = I_{AC}(-\tau). \tag{2.10}$$

Note that the phase of the pulse in the time domain is completely washed out in the measurement and intensity autocorrelation only provides information on the pulse intensity. If the pulse shape is known, the pulse width can be retrieved by deconvolution of the autocorrelation function, where the temporal pulse duration is given by dividing the autocorrelation signal by the deconvolution factor. Examples of deconvolution factors for common pulse shapes are listed in table 2.2.

Table 2.2. *Deconvolution factors for different pulses*

Pulse shape	**Deconvolution factor**
Sech^2	0.647
Gaussian	0.707
Rectangular	1
Triangular	0.692

Retrieving the pulse width for complex pulse shapes using intensity autocorrelation can be problematic since different pulse shapes can yield similar autocorrelation traces[15]. In particular, it has been shown that the autocorrelation trace approaches a narrow spike sitting on top of a broad pedestal as the pulse intensity becomes increasingly complex [16].

2.3.4 Interferometric autocorrelation

Interferometric autocorrelation (also called phase-sensitive autocorrelation and fringe-resolved autocorrelation (FRAC)) is a pulse characterization method that also provides information of the pulse phase. The input beam is split into two similarly to the case of intensity autocorrelation and one of them is delayed. The main difference is that the pulses are sent colinearly to the nonlinear crystal. Due to coherent addition of the two beams, interference occurs and interference fringes are observed as the delay is applied. An illustration of interferometric autocorrelation measurement setup in fig 2.6 where nonlinear interaction is used to produce the interference signal. Alternatively two-photon absorption

directly in the detector can also be used.

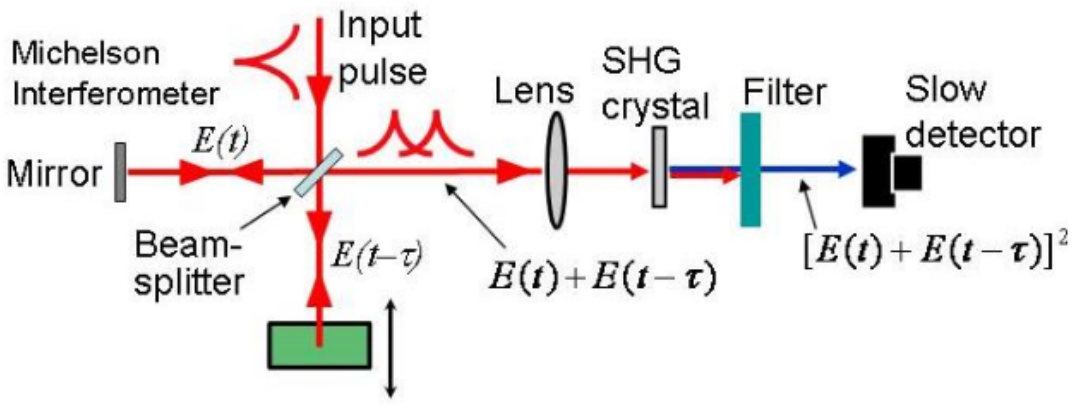

Figure 2.6. *Principle of interferometric autocorrelation with filtered SHG [14]*

The expression for interferometric autocorrelation trace is given by

$$I_{IAC}(\tau) = \int_{-\infty}^{\infty} |[E(t)E(t-\tau)]^2|^2 dt \tag{2.11}$$

$$I_{IAC}(\tau) = \int_{-\infty}^{\infty} |E(t)^2 + 2E(t)E(t-\tau) + E(t-\tau)^2|^2 dt. \tag{2.12}$$

Expanding this further leads to the following expression:

$$I_{IAC}(\tau) = I_{back} + I_{AC} + I_{\omega} + I_{2\omega}, \tag{2.13}$$

where

$$I_{back} = 2\int_{-\infty}^{\infty} I(t)^2 dt \tag{2.14}$$

$$I_{AC}(\tau) = 4\int_{-\infty}^{\infty} I(t)I(t-\tau)dt \tag{2.15}$$

$$I_{\omega}(\tau) = 4\int_{-\infty}^{\infty} Re[(I(t)+I(t+\tau))E^*(t)E(t+\tau)e^{j\omega\tau}]dt \tag{2.16}$$

$$I_{2\omega}(\tau) = 2\int_{-\infty}^{\infty} Re[E(t)^2E^*(t-\tau)^2e^{j2\omega\tau}]dt. \tag{2.17}$$

As seen in equation 2.13 the IAC trace consists of four different terms: constant background, Intensity autocorrelation, coherence term oscillating with ω_c and coherence term oscillating with $2\omega_c$ (ω_c being the center wavelength of the incoming pulse). Equation 2.13 is often normalized with respect to the background intensity I_{Back} yielding normalized interferometric autocorrelation trace

$$I_{IAC}(\tau) = 1 + \frac{I_{AC}(\tau)}{I_{Back}} + \frac{I_{\omega}(\tau)}{I_{Back}} + \frac{I_{2\omega}(\tau)}{I_{Back}}. \tag{2.18}$$

By filtering out the oscillating terms I_ω and $I_{2\omega}$, the IAC signal reduces to the intensity autocorrelation signal with constant background of 1 as seen in equation 2.18. This is clear from 2.13 that IAC provides extra information compared to intensity autocorrelation.

The IAC has similar symmetrical property as the intensity autocorrelation $I_{IAC}(\tau) = I_{IAC}(-\tau)$. At zero delay ($\tau$=0) all integrals are identical:

$$\begin{aligned} I_{back} &= 2\int_{-\infty}^{\infty} I(t)^2 dt \\ I_{AC}(\tau=0) &= 4\int_{-\infty}^{\infty} I(t)I(t)dt = 2I_{back} \\ I_{\omega}(\tau=0) &= 4\int_{-\infty}^{\infty} Re[(I(t)+I(t+0))E^*(t)E(t+0)e^{j\omega*0}]dt = 4I_{back} \\ I_{2\omega}(\tau=0) &= 2\int_{-\infty}^{\infty} Re[E(t)^2E^*(t-0)^2e^{j\omega*0}]dt = I_{back}. \end{aligned}$$

And we obtain

$$I_{IAC}(0) = I_{IAC}(\tau)|_{max} = 8. \tag{2.19}$$

Also IAC signal have properties of

$$I_{IAC}(\tau \to \infty) = 1 \tag{2.20}$$

$$I_{IAC}(\tau)|_{min} \to 0 \tag{2.21}$$

As seen in the Eqs 2.19-2.21 the wings of the IAC signal decays towards a constant background of 1, the maximum of the signal is 8 at zero delay and the minimum is reached at delay corresponding to opposite phase of the interfering pulses near the zero delay position. This background to peak ratio 1:8 is important for IAC and it can be used to verify proper alignment of the setup as this ratio is not achieved if the interfering beams are not precisely colinear [16].

3 EXPERIMENTAL SETUP

The experimental setup used in the measurements is shown in figure 3.1. The drtup includes Ti:sapphire laser to generate short intense pulses, an optical isolator to prevent back reflections, a fiber that generates supercontinuum and a Michelson interferometer and TPA detector that allows performing interferometric autocorrelation measurements.

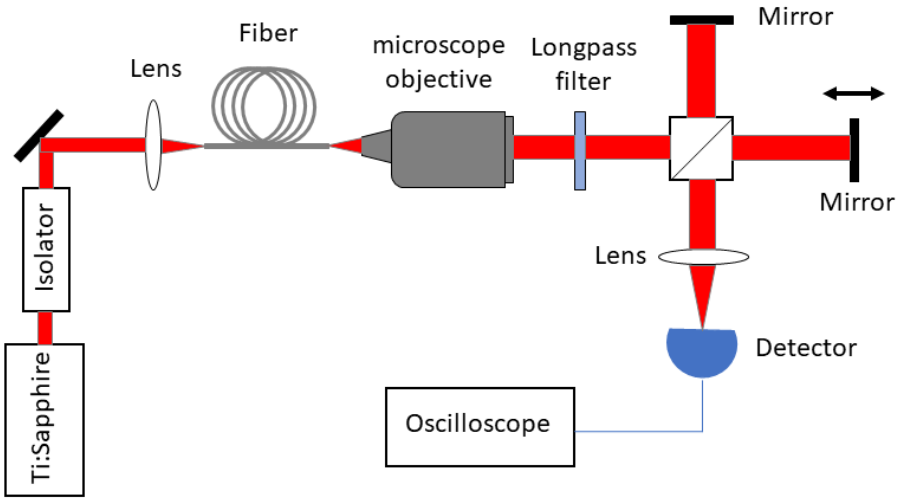

Figure 3.1. *Experimental measurement setup.*

First 200fs pulses at 80MHz repetition rate and central wavelength of 860nm from the Ti:sapphire laser (Spectra-Physics Tsunami) were directed through an optical isolator (Thorlabs IO-5-NIR-LP). The isolator was used to avoid excess of back reflections from the setup to the laser. Back reflections are mainly caused by Fresnel reflection from the air-silica interface when light is injected into the fiber. The isolator is an important part of the laser stability since back reflections can affect significantly the mode-locking operation of the laser.

After passing through the isolator the beam is coupled into the fiber using an aspheric lens. The numerical aperture (NA) of the lens was 0.43, which is close to that of the fiber. Although the aperture of the lens was not completely filled with the beam. Other combinations of lenses and beam sizes were tested and this particular set was found to be optimal, yielding a coupling efficiency of 70%.

At the fiber output, the beam was collimated using a microscope objective (Nikon LU Plan Fluor). The objective was chosen because it is corrected for chromatic aberration in the near-infrared. Both input tip of the fiber and the collimating objective were attached to XYZ-translation stages (Thorlabs NanoMax-TS and MBT616) to optimize coupling and collimation of the beam. A long pass filter was inserted after collimation to block wavelengths unsuitable for two-photon absorption detection.

After supercontinuum was generated and filtered in a proper way, light was guided to the Michelson interferometer which consists of a beam splitter, two mirrors at the end of both arms and the detection part. In the interferometer the beam was split between the two arms using a non-polarizing 50:50 beamsplitter cube with near-infrared coating. In both arms light is reflected back with mirrors. one of the arm has a stationary mirror while the other is attached to an electrically driven translation stage (Newport AG-LS25) which allows to tune the delay between two arms. Comapred to conventional Michelson interferometer, detection is achieved using two-photon absorption. To maximize the TPA signal, the beam was focused to the detector using an aspheric lens with NA of 0.5. An amplified GaP semiconductor photodiode (Thorlabs PDA25K) connected to a 2MHz oscilloscope (LeCroy WaveRunner 204Xi) was used to record the signal from the interferometer for different delays.A labview program was used to control and vary the delays.

3.1 The optical fiber

The optical fiber used to generate the supercontinuum was a 56cm long highly nonlinear photonic crystal fiber with zero dispersion wavelength of 850nm (Thorlabs NL-2.8-850-02). The fiber is designed to generate a supercontinuum in the NIR region and it is suitable for Ti:sapphire or diode pumped Nd^{+3} lasers[17].

Figure 3.2 shows the cross-section of the fiber. It is the simplest and most widespread structure of PCFs. In the middle of a silica cladding is a triangular pattern of air holes, with one hole missing in the center. The effective refractive index in the region of the missing hole is higher than that in the holes area thus behaving like the core in conventional fibers. This kind of structure is resulting in strong confinement of the light and correspondingly efficient nonlinear effects[18].

According to the manufacturer of the fiber, the distance between the cladding holes is 2.7μm and the core diameter 2.8μm. The diameter of the holey region and outer silica

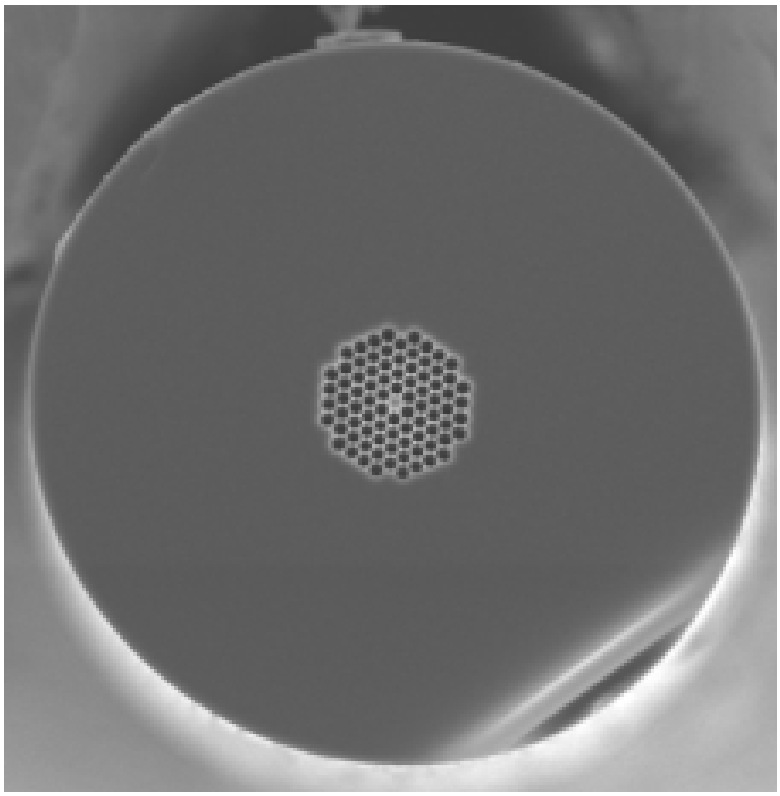

Figure 3.2. *Picture of the PCF fiber used for generating the SC[17].*

cladding are 28μ and 136μm, respectively.

In the experiment, the Ti:sapphire laser was tuned to the center wavelength of 860nm to inject pulses in the PCF above its zero dispersion wavelength (anomalous dispersion regime) allowing to achieve significant spectral broadening. One example of SC spectrum generated before and after the long pass filter is shown in figure 3.3. The spectrum spans roughly from 550nm to 1300nm. Wavelengths below 750nm hwere filtered out with the long-pass filter as discussed in the detection system part below.

3.2 Delay stage

A translation stage (Newport Ag-LS25) driven by piezo motion control (Newport AG-UC2) was used to change the delay between the two arms in the Michelson interferometer. The stage is not closed loop and does not provide feedback on the movement. It can be translated by feeding step amplitude corresponding to a specific current value. The step amplitude is not directly related to the actual step size by which the stage is really moving. The workload on top of the stage and even the position in the stage can affect the step size. It can also vary even when step amplitude is set to same amount and position in the stage is the same between different measurements. The step amplitude was set to the lowest possible value to achieve maximum precision in the measurements.

The step size must to be estimated separately for the used step amplitude. One approach

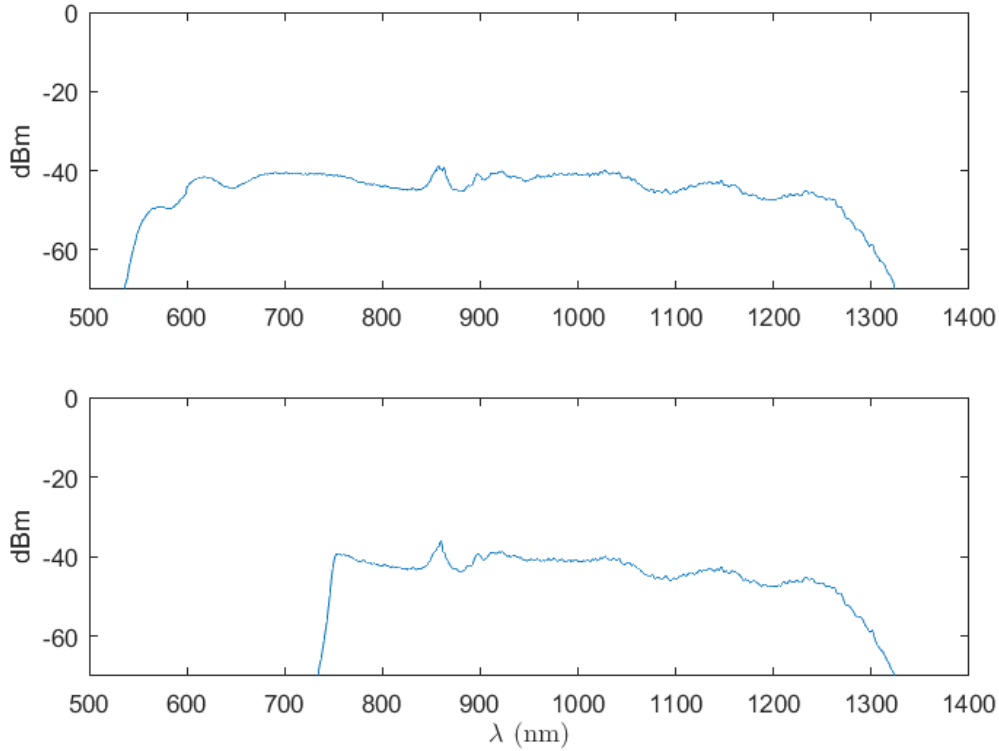

Figure 3.3. *Measured supercontinuum spectrum with input power of 300mW without (upper) and with (lower) long pass filter. Used pump wavelength was 860nm*

is to scan the entire range of the stage (1.2cm) and measure the number of steps in this interval. Dividing the distance by the number of steps, one gets an average estimation of the step size. Another more accurate approach is to use the Michelson interferometer. By measuring light of Ti:sapphire with known wavelength with different delays, step size of the stage can be resolved since oscillations in the measured data corresponding to the wavelength of the light as discussed in the results section. The average step size was calculated to be 60nm

3.3 Detection system

The detection system in the measurements consisted of a focusing aspheric lens and amplified GaP semiconductor photodiode (Thorlabs PDA25K) attached to the 2MHz oscilloscope (LeCroy WaveRunner 204Xi). The detector has high gain transimpendance amplifier with 8 different gain positions in 10dB steps and up to 70dB. A rotating knob on the side of the detector is used to control the gain.

The detector responsivity for different wavelengths is shown in figure 3.4. The detection range is roughly from 150nm to 550nm which makes the photodiode suitable for detecting two-photon absorption (TPA) from 700nm to 1100nm. Even though the linear absorption is very weak above 550nm, the tail still extends towards the longer wavelengths. Since

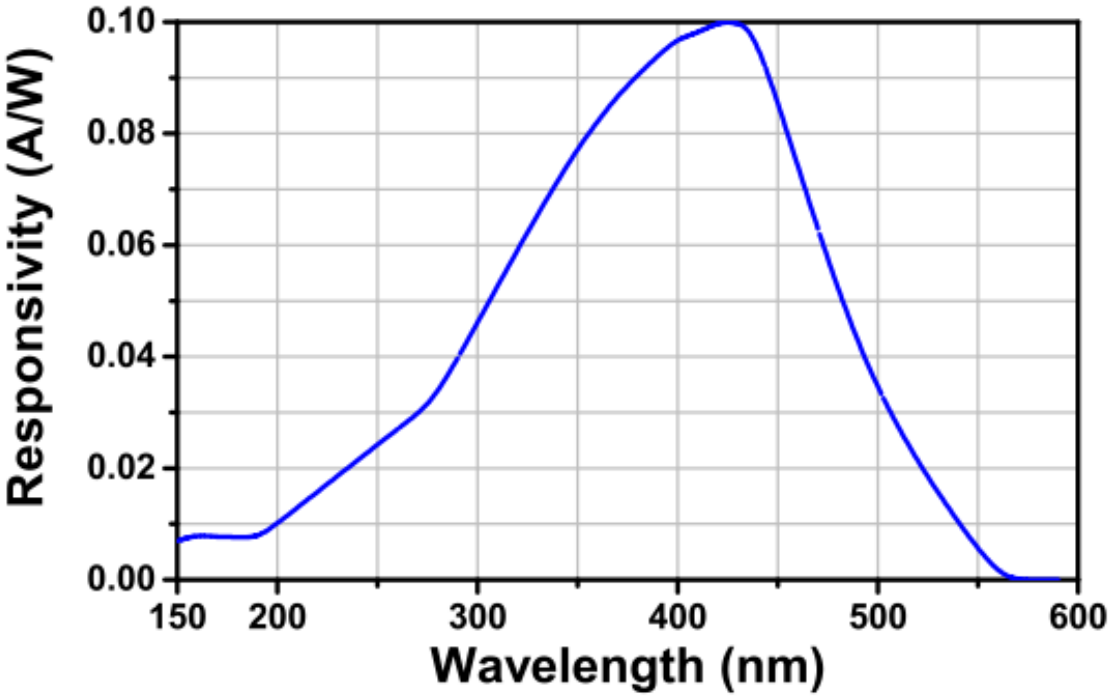

Figure 3.4. *Detectors responsivity vs. wavelength [19].*

two-photon absorption is several magnitudes weaker, the tail is still playing an important role and the detector is not suitable for detecting TPA between 550nm and 700nm.

As we are only interested in measuring TPA, the detector clearly limits the measurement since the supercontinuum spectrum extends below the detector TPA limit into the single-photon absorption regime. In order to circumvent this limitation, the supercontinuum was filtered with a long pass filter.

Before characterizing supercontinuum ligths, the detector ability to detect TPA was tested using light only from the Ti:sapphire laser at different wavelengths in the 700nm- 1000nm range. The fraction of two-photon and single-photon absorption can be measured by increasing the power and monitoring the dependency in the measured signal. As the TPA is proportional to the intensity squared, the signal measured by the detector scales to the power squared if the beam size remains unchanged. By plotting signal versus power in logarithmic scale, the rate of change corresponds to the power dependency. TPA dominates when the slope is two and everything between one and two is a mix of the linear and nonlinear signal. An example of this is plotted in figure 3.5 at the wavelength of 800nm.

Table 3.1 summarizes the slopes of the logarithmic plot for different wavelengths. From the slope values it can be seen that TPA is dominating for wavelengths above 750nm, and a longpass filter 750nm for the supercontinuum measurements was therefore selected. The slope value higher than two for the wavelength of 1000nm might be caused by three-photon absorption. Adding a short pass filter below 1000nm was also tested for the

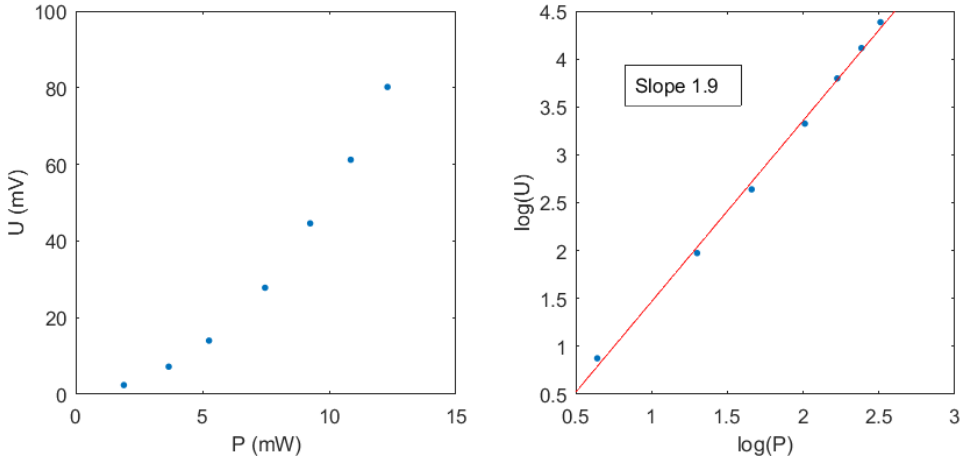

Figure 3.5. *Measured signal plotted with respect to power in linear (left) and logarithmic (right) scale from Ti:sapphire pulses at a wavelength of 800nm. A 10dB gain was used in the detector.*

supercontinuum characterization but no difference was observed.

Table 3.1. *Power dependency of the detected signal from Ti:sapphire pulses for different wavelengths.*

λ **(nm)**	**slope**
700	1.74
750	1.98
800	1.9
850	2
900	1.9
950	2
1000	2.18

An aspheric lens with NA 0.5 was used to focus light as tight as possible to maximize two-photon signal in the detector. The diameter of the lens was chosen to fit the beam size of the collimated supercontinuum for optimal focus. Also, achromatic lenses and microscope objectives were tested to optimize TPA. Achromatic lenses correct chromatic aberration and thus focusing different wavelengths better to the same spot on the detector. However, focusing is not as tight as with aspheric lens yielding less TPA signal. High NA microscope objectives instead would decrease spot size in the focus. Nevertheless, since detectors light-sensitive semiconductor layer is a couple of mm inside, it limits the focal length and thus no improvement was achieved with the microscope objective.

4 RESULTS

First we tested the IAC measurement setup with the short pulses emitted by the mode-locked Ti:Sapphire laser. The measured interferometric autocorrelation and filtered intensity autocorrelation traces are shown in figure 4.1. The signal maximum and minimum approaches 8 at zero delay and 0 near zero delay, respectively which indicated that the interferometer is well-aligned (Chapter 2.3.4). Also the signal decays to unity at long delay values as expected. From the signal it is also visible that interference are not observed across the full delay over which the delayed pulses overlap. This is caused by the chirp in the input pulse that is induced by the dispersion caused by the optical isolator and other optical components in the setup.

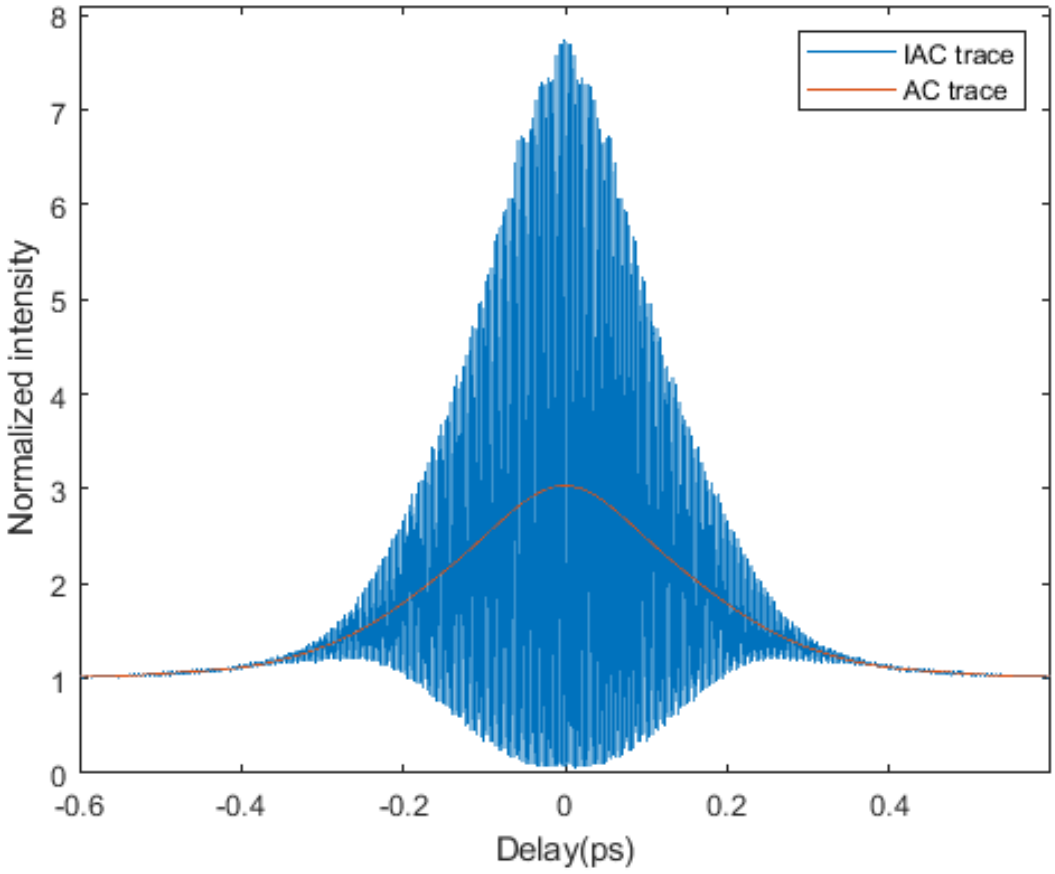

Figure 4.1. *IAC and filtered AC traces from the mode-locked Ti:Sapphire laser*

The intensity autocorrelation trace is obtained by filtering the fast oscillating components

from the IAC signal. Filtering is achieved by taking The Fourier transform of the IAC and removing the low-frequency components around the 0 frequency in the spectrum. Taking the inverse Fourier transform of the filtered signal then yields the AC trace. Figure 4.2 shows the spectrum before and after filtering operation. The Intensity of the spectrum is displayed in logarithmic scale. On the top figure outermost peaks corresponds to 2ω and middle peaks to ω as is presented in equation 2.18 (Chapter 2.3.4). The width of the autocorrelation trace was found the be $\sim$320 fs which corresponds to $\sim$210 fs duration by assuming hyperbolic-secant shape with deconvolution factor of 0.647 (see table 2.2 in Chapter 2.3.3).

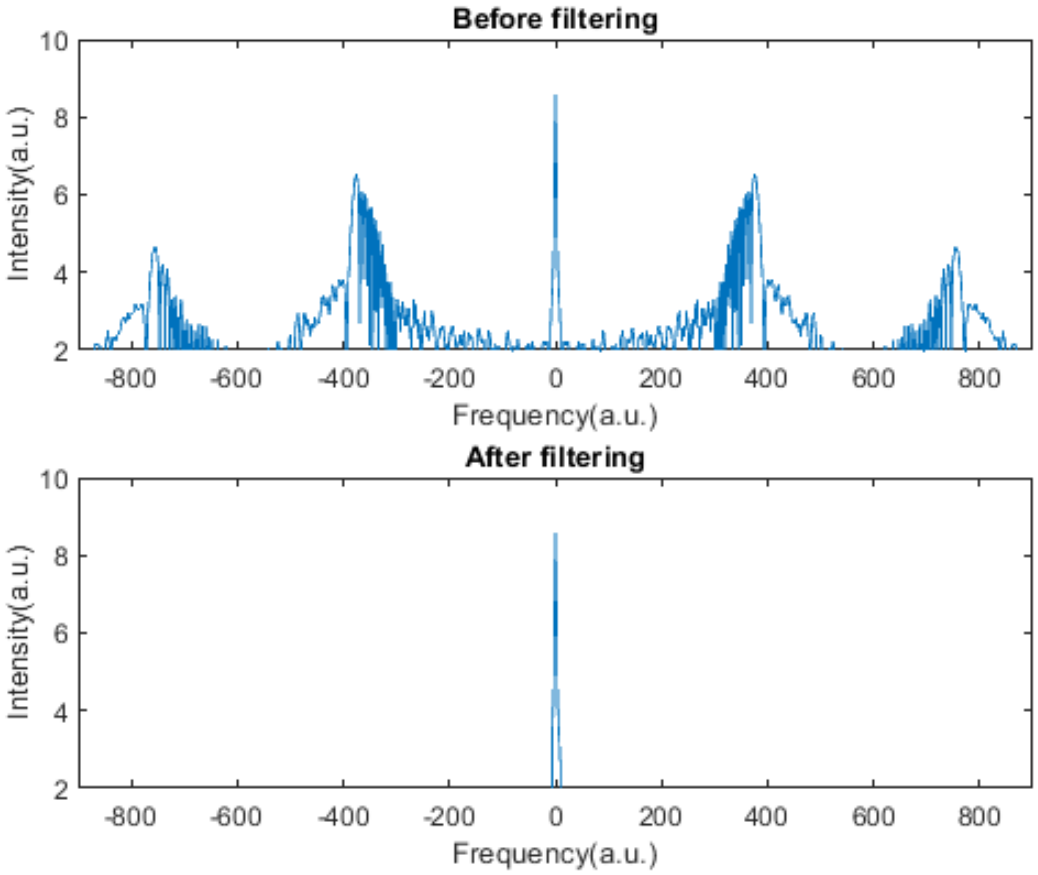

Figure 4.2. *IAC spectrum from the Ti:Sapphire laser before and after filtering fast oscillation components at 2ω (outermost) and ω around the center peak. Intensity is in logarithmic scale*

Next supercontinuum light described in chapter 3 was analyzed with the interferometer. Figure 4.3 illustrates the IAC trace of the supercontinuum. It is also seen that alignment is good since the signal reaches values close to zero with zero delay. However typical maximum of 8 is not reached at the zero delay. This is because two-photon absorption is not fully dominating the absorption process and linear absorption occurs in the detector. This was not problem with the laser light as the spectrum was restricted to near half of the bandgap energy. In the supercontinuum case however the spectrum expands to shorter

wavelengths and the detector is more sensitive for linear absorption at these wavelengths. In the conclusion section, we provide a possbiel path to overcome this problem.

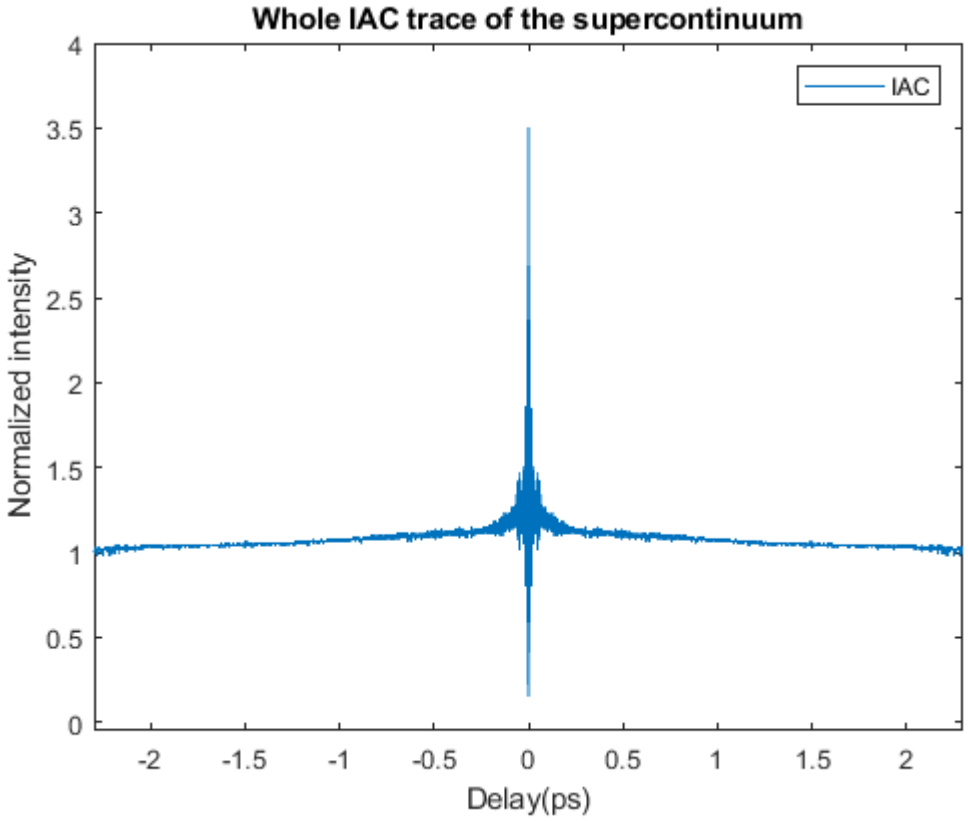

Figure 4.3. *Whole IAC trace of the supercontinuum*

The portion of the IAC trace zoomed near the zero delay is presented in fig 4.4. Oscillations are observed in the center and also coherent sub-structures around the main peak. The AC trace is also presented in the same figure and is obtained similarly as above by taking Fourier transform from IAC and filtering ω and 2ω around the center frequency and returning to time-domain by inverse Fourier transform.

The full AC trace is shown in figure 4.5. The AC trace reaches background around a delay of 2ps indicating that the supercontinuum pulses spam at least 2ps duration on average. Also a sharp peak in the zero delays is observed on top of pulse like pedestal. This kind of structure is typical for chaotic light and gives indication that the supercontinuum light measured is not fully coherent [20]. Although specific intensity values of the pedestal and peak is needed for analysis to compare with simulations and other light sources. Since nonlinear signal is not only shown in the IAC trace conclusions of how high values AC peak reaches cannot be drawn.

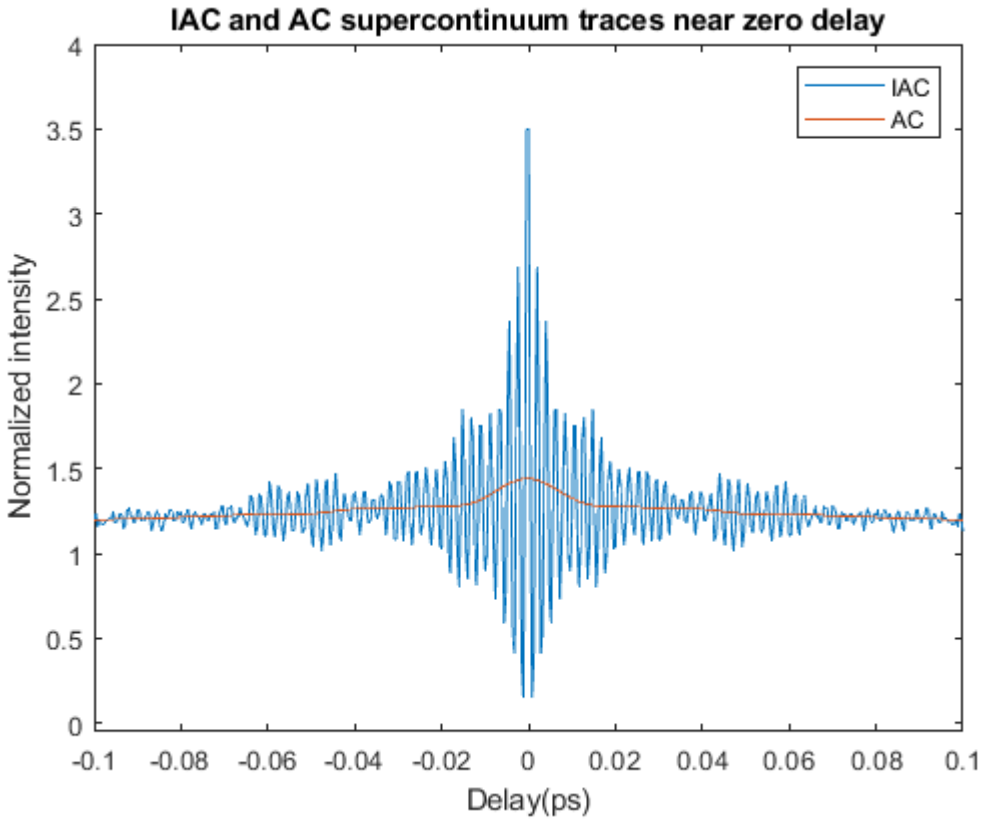

Figure 4.4. *Zoom near zero delay of the supercontinuum IAC trace*

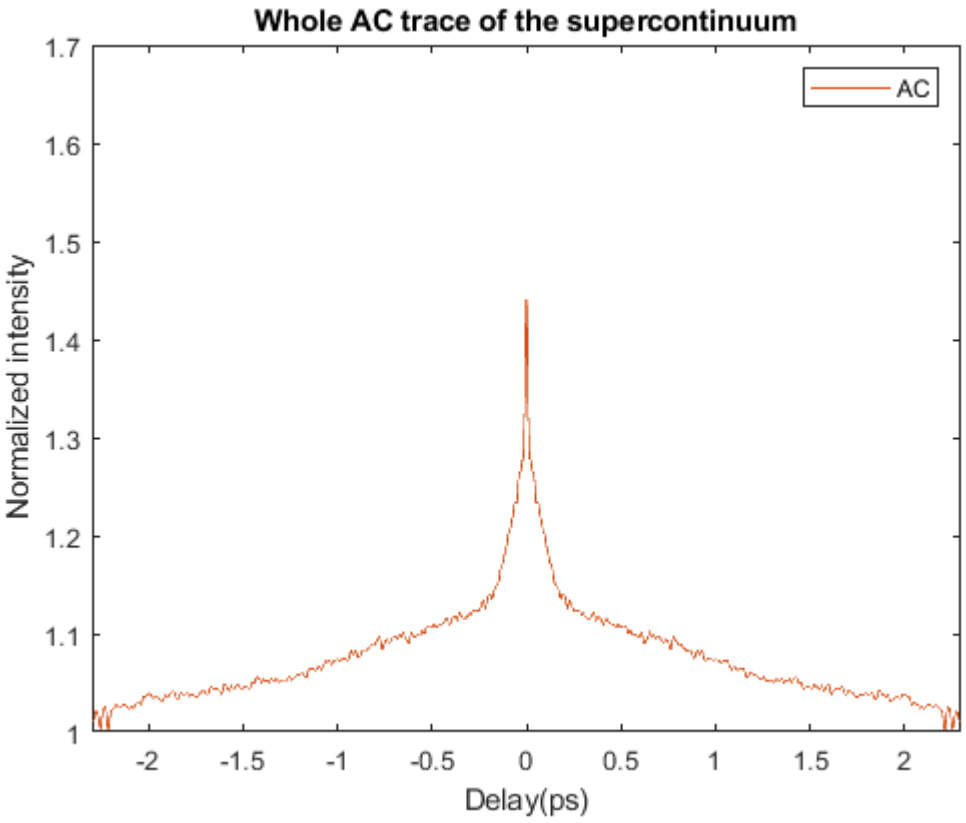

Figure 4.5. *Full AC trace of the supercontinuum*

5 CONCLUSION

In this thesis, a technique based on interferometric autocorrelation with two-photon absorption was used to obtain qualitative information about intensity correlation of supercontinuum light. Two-photon absorption is essential for measurement with supercontinuum as compared to the more conventional second-harmonic generation based interferometric measurements since two-photon absorption enable measuring very broad spectrum without phase matching constrains.

The retrieved IAC trace showed the residual presence of linear absorption in the measured signal, arising most likely from impurities in the semiconductor material of the detetor. Therefore to overcome this problem next step for the measurement is proposed. Linear absorption and non-linear absorption are independent of each other so it is possible to measure IAC trace also without focusing the light to the detector and thereby measuring only linear absorption. This linear absorption can then be subtracted from the IAC trace which have both linear and nonlinear absoprtion to yield the true IAC trace.

Scanning through delays with focus and after that scanning out of focus is not practical since points have to be measured at the exactly same delay steps and this would require impractical precision and ability to repeat from the delay stage. However placing additional electrically controlled stage to focus and unfocus light to detector during scanning in the same delay steps seems to be a robust solution.

REFERENCES

[1] Dorsinville R. Ho P. Manassah J., A. R. *The supercontinuum Laser Source*. Springer, 2006.

[2] Dudley, J. M. and Coen, S. Coherence properties of supercontinuum spectra generated in photonic crystal and tapered optical fibers. *Opt. Lett.* 27.13 (2002), 1180–1182.

[3] Saleh, B. and Teich, M. *Fundamentals of Photonics*. John Wiley Sons, Ltd, 2001. Chap. 8, 272–309.

[4] Travers, J. C., Frosz, M. H. and Dudley, J. M. *Nonlinear fibre optics overview*. Ed. by J. M. Dudley and J. R. Taylor. Cambridge University Press, 2010, 32–51.

[5] Boyd, R. W. *Nonlinear Optics (Fourth Edition)*. Ed. by R. W. Boyd. Fourth Edition. Academic Press, 2020.

[6] Mollenauer, L. F. and Gordon, J. P. *Solitons in Optical Fibers*. Burlington: Academic Press, 2006.

[7] Aßmann, M. and Bayer, M. *Quantum Optics with Semiconductor Nanostructures*. Ed. by F. Jahnke. Woodhead Publishing, 2012, 154–185.

[8] Hunt, M., Taverne, M., Askey, J., May, A., Van Den Berg, A., Ho, Y.-L. D., Rarity, J. and Ladak, S. Harnessing Multi-Photon Absorption to Produce Three-Dimensional Magnetic Structures at the Nanoscale. *Materials* 13.3 (2020).

[9] Rumi, M. and Perry, J. W. Two-photon absorption: an overview of measurements and principles. *Adv. Opt. Photon.* 2.4 (2010), 451–518.

[10] Loudon, R. *The Quantum Theory of Light*. Oxford: Clarendon Press, 1973.

[11] Wikipedia. *Hanbury Brown and Twiss effect*. URL: https://en.wikipedia.org/wiki/Hanbury_Brown_and_Twiss_effect.

[12] Ulrich, S. M. *Non-Classical and Stimulated Photon Emission Processes from Self-Assembled Semiconductor Quantum Dots*. Verlag Dr. Hut, 2007.

[13] Scully, M. O. *Quantum optics*. Cambridge: Cambridge University Press, 1997.

[14] SwampOptics. *Interferometric autocorrelation*. URL: http://www.swampoptics.com/autocorrelation.html.

[15] Chung, J.-H. and Weiner, A. M. Ambiguity of ultrashort pulse shapes retrieved from the intensity autocorrelation and the power spectrum. *IEEE Journal of Selected Topics in Quantum Electronics* 7 (2001), 656–666.

[16] Trebino, R. and Zeek, E. *Frequency-Resolved Optical Gating: The Measurement of Ultrashort Laser Pulses*. Boston, MA: Springer US, 2000, 61–99.

[17] Thorlabs. *Highly nonlinear photonic crystal fiber*. URL: https://www.thorlabs.com/thorproduct.cfm?partnumber=NL-2.8-850-02&pn=NL-2.8-850-02.

[18] RP-photonics. *Photonic Crystal Fibers*. URL: https://www.rp-photonics.com/photonic%5C_crystal%5C_fibers.html.

[19] Thorlabs. *Free-Space Biased Detectors*. URL: https://www.thorlabs.com/newgrouppage9.cfm?objectgroup_id=1295.

[20] Toenger, S., Makitalo, R., Ahvenjarvi, J., Ryczkowski, P., Narhi, M., Dudley, J. M. and Genty, G. Interferometric autocorrelation measurements of supercontinuum based on two-photon absorption. *J. Opt. Soc. Am. B* 36.5 (2019), 1320–1326.